Hydrodynamics of Trickle-Bed Reactors: Experiments and CFD Modeling

Prashant R. Gunjal, Madhavanand N. Kashid, Vivek V. Ranade,* and Raghunath V. Chaudhari

Industrial Flow Modeling Group, Homogeneous Catalysis Division, National Chemical Laboratory, Pune 411008, India

Hydrodynamics of trickle-bed reactors involve complex interactions of gas and liquid phases with packed solids. Such complex interactions manifest in different flow regimes occurring in trickle-bed reactors. Knowledge of prevailing flow regime, pressure drop, and liquid holdup is essential for design and performance evaluation of the reactor. Detailed knowledge of fluid dynamics is essential for "a priory" predictions as well as for interpretation of available data. In this study, we have used wall pressure fluctuation measurements to identify prevailing flow regime in trickle beds. Experiments were carried out on two scales of columns (of diameter 10 cm and 20 cm) with two sets of particles (3 mm and 6 mm diameter spherical particles). Effects of prewetted and unwetted bed conditions on pressure drop and liquid holdup were reported for a range of operating conditions ($V_G = 0.22-0.44$ kg/m^{2}s, $V_L = 2-24$ kg/m^{2}s). A comprehensive CFD model was developed to predict measured hydrodynamic parameters. The model was evaluated by comparing predictions with the experimental data. The CFD model was then extended to predict the fraction of liquid holdup suspended in the form of drops in the bed. At the end, the CFD model was used to understand hydrodynamics of trickle beds with periodic operation. The experimental data as well as computational models discussed here will have significant implications for understanding and designing of trickle-bed reactors.

Introduction

Trickle-bed reactors (TBR) are widely used in chemical process industries because of their flexibility and simplicity in operation for low as well as high throughputs. In trickle-bed reactors gas and liquid phases flow co-currently downward through a fixed bed of catalyst particles. Under commonly used operating conditions, gas flows as a continuous media while liquid trickles over solid particles. A trickle-bed reactor behaves close to plug flow for gas as well as for liquid phases and has smaller liquid holdup (higher solid holdup) compared to the slurry and ebullating bed reactors. The typical applications of trickle-bed reactors include hydrocracking, hydro-desulfurization, and hydro-denitrogenation of gas oil, catalytic dewaxing of gas oil and lube oils, oxidation and hydrogenation of organic compounds, and wastewater treatment. Accurate understanding of hydrodynamics of trickle-bed reactors and knowledge of how it changes with key design (particle and reactor diameter, distributor, and so on) and operating parameters (gas and liquid flow rates, periodic operation, and so on) are therefore essential. Several studies have been carried out to understand and to quantify hydrodynamics of trickle-bed reactors. In this work, we report results of detailed investigation of hydrodynamics of trickle-bed reactors using experimental as well as computational tools. The physical picture of gas−liquid flow through a trickle bed and review of previous studies are briefly discussed in the following sections.

* To whom correspondence should be addressed. E-mail: vvranade@ifmg.ncl.res.in.

Physical Picture and Flow Regimes in Trickle-Bed Reactors. When gas and liquid flow co-currently downward through a packed bed of solid particles, several flow regimes were found to occur depending upon operating and design parameters. When gas and liquid flow rates are small, liquid flows down in the form of a film over a solid surface. This regime is called a film flow [see Figure 1A(a)] in which both phases are continuous (or semicontinuous). In this regime, depending on the liquid flow rate, the solid surface may be completely or partially wetted. At low liquid flow rates, if the gas flow increases, interaction of the gas phase with liquid film flowing over a solid surface increases. Eventually, at certain gas velocity, gas starts entraining part of the liquid. Thus, under such a condition, part of the liquid flows down in the form of suspended droplets in the gas phase and part of the liquid flows down in the form of film over a solid surface [like in Figure 1A(b)]. This regime is called trickle flow regime. More often than not, the film flow regime is also clubbed with the trickle flow regime. If the gas flow rate increases further, a stage may come when all the liquid flows down in the form of suspended droplets. This regime is called a spray flow regime [see Figure 1A(c)]. When the liquid flow rate is increased at high gas velocity, two distinct gas and liquid rich bands (pulses) flow downward through the packed bed. This regime is called a pulse flow regime. If the liquid flow rate is increased further, a stage comes when gas becomes a dispersed phase [see Figure 1A(d)] and flows down in the form of bubbles. This regime is called a bubbly flow regime.

A typical flow regime map for a trickle-bed reactor is shown in Figure 1B (taken from Sie and Krishna[1]). Out

10.1021/ie0491037 CCC: $30.25
Published on Web 02/23/2005

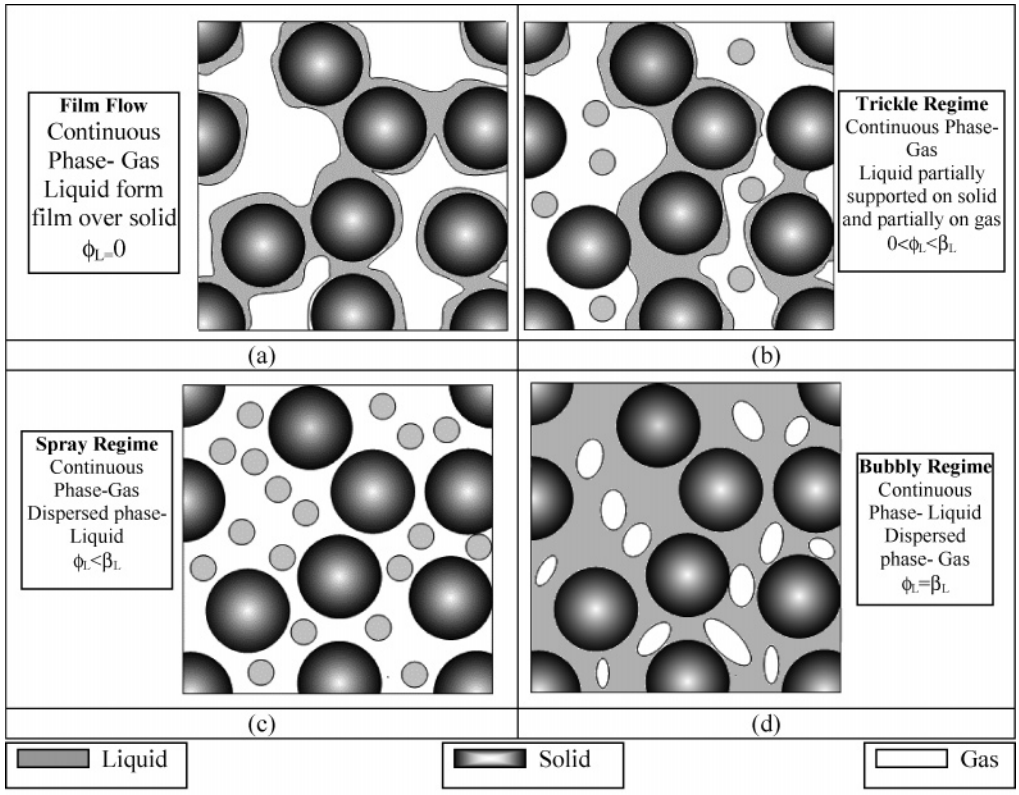

(A) Physical Picture of the Flow in Trickle Bed Reactors

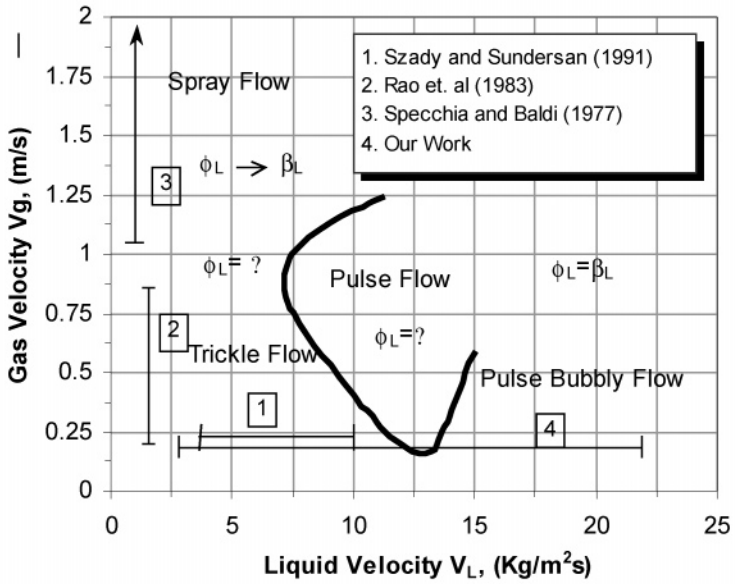

(B) Flow regime map (Sie and Krishna[1])

Figure 1. Gas−liquid flow regimes in a packed-bed reactor.

of these flow regimes, most of the trickle-bed reactors are operated in trickle and pulse flow regimes. Flow characteristics in these regimes are extremely complex and associated with the interaction of the fluids in the bed. For example, in a trickle flow regime, spreading of liquid over the catalyst surface is controlled by the nature of the solid surface and its dry or wetted condition. In a pulse flow regime, pulse formation, pulse frequency, and holdup affect the hydrodynamic characteristics. Identification of different flow regimes and knowledge of their flow characteristics are essential because other transport processes such as heat- and mass-transfer rates are dependent on flow regimes and extent of interaction among gas, liquid, and solid phases. Knowledge of how flow regimes and key hydrodynamic parameters are influenced by design and operating parameters is also essential for scale-down (designing laboratory experimental setup and experiments) and for scale-up (using laboratory experimental data for designing industrial reactors). Previous studies on these aspects are briefly reviewed in the following.

Previous Work. Most of the experimental studies on trickle-bed hydrodynamics were restricted to trickle and pulse flow regimes. Several ways have been used to identify flow regime transition from trickle to pulse. Latifi et al.[2,3] have used a microelectrode technique to determine the flow regime transition in trickle-bed reactors. However, detailed information on frequency distribution in a pulse flow regime has not been reported. In recent years, nonlinear time series analysis has been extensively used to characterize flow regime transitions in bubble columns and fluidized-bed reactors (see, for example, Drahos et al.,[4] Letzel et al.,[5] and Lin et al.[6]). Relatively few attempts have been made to use these techniques for identifying flow regime transitions in trickle-bed reactors. Krieg et al.[7] studied flow regimes in trickle beds with wall pressure fluctuations and power spectral density (PSD). Their study indicated that visual techniques are not able to capture regime transitions accurately. They used variation in pressure fluctuations and conductance values to identify regime transition. Horowitz et al.[8] have used nonlinear time-series analysis tools such as rescaled range analysis and correlation dimension to find the flow regime transition. Recently, Urseanu et al.[9] have identified flow regime transition based on standard deviation in pressure drop. However, this technique could not give sharp boundary at which transition occurs. It is essential to develop easy to use techniques to identify flow regime transitions in trickle-bed reactors.

A large number of studies were carried out for measurement of pressure drop and liquid holdup in trickle beds (see, for example, Al-Dahhan et al.,[10] Saez and Carbonell,[11] Herskowitz and Smith,[12] and references therein). However, studies which addressed effect of prewetted and nonprewetted bed conditions on pressure drop/liquid holdup (and their hysteresis) are rather few. The hysteresis of pressure drop and liquid holdup in trickle beds was first observed by Kan and Greenfield.[13,14] They explained the phenomenon based on the formation of liquid bridges and surface tension. Christensen et al.[15] and Levec et al.[16,17] observed that the radial distribution of the liquid in the bed changes depending on whether the liquid flow rate increases or decreases and stated it as a cause for hysteresis. Rode et al.[18] have also reported multiple hydrodynamics states in various flow regimes of trickle-bed reactors. Chu and Ng[19] modeled the packed bed by arranging the packing in a cubical structure and considered the lower branch of hysteresis as filament flow with the upper branch as film flow. Ravindra et al.[20] reported experimental data on hysteresis by reconciling the previous results. Melli and Scriven[21] studied hysteresis theoretically in a two-dimensional bed. It is however necessary to obtain systematic experimental data to understand and to quantify hysteresis in trickle beds. Such a systematic data set is also needed for evaluating computational models of gas−liquid flow through trickle beds.

In recent years, computational fluid dynamics (CFD) based models are showing promising results for a variety of complex reactors. Several efforts are being made to develop computational flow models for trickle-bed reactors. Attou and Ferschneider[22] have developed a one-dimensional flow model for prediction of global hydrodynamic parameters. Because it is one-dimensional, their model cannot take account of radial variation in bed porosity. Jiang et al.[23] have developed a two-dimensional CFD model including variation of bed porosity. This model was able to capture some of the key features of hydrodynamics of trickle beds. Iliuta et al.[24] and Souadnia and Latafi[25] have used the CFD model for predicting hydrodynamics characteristics over a wide range of operating parameters. Gunjal et al.[26] have used a similar CFD model for studying liquid-phase mixing and liquid distribution. However, both of these studies were restricted to trickle flow regime. None of the CFD models published so far were used to simulate spray or pulse regimes or to simulate the observed hysteresis on pressure drop.

Simulation of pulse flow regime requires a detailed understanding of complex interactions of liquid spreading on a solid surface, capillary forces, and gas flow. Though underlying physics of such complex flows is not completely understood, computational models may shed some light on such complex flows. Recently, Professor Dudukovic and his group initiated CFD modeling of periodic operation of trickle beds (private communications). This approach may be extended to understanding differences and similarities between periodic operation (liquid-rich−gas-rich feed) and pulse flow regime. For simulating spray flow regime, it is necessary to develop ways of estimating the fraction of liquid suspended in the gas phase. The observed pressure drop in trickle beds can be related to flow frictional pressure drop as

$$\left(\frac{dP}{L}\right)_F = \left(\frac{dP}{L}\right)_{obs} + \rho_G g \beta_G + \rho_L g \beta_L \theta_L \qquad (1)$$

where β_G and β_L are the gas and liquid saturation, respectively. θ_L is the fraction of liquid suspended in the gas phase in the form of droplets. Considering the small magnitude of gas density, the second term of the right-hand side is usually neglected. In trickle beds, depending upon operating regime, the fraction of liquid suspended in the gas phase varies from 0 to 1. In the film flow regime, all the liquid flows in the form of film and the fraction of liquid suspended in the gas phase is zero. In such a case, frictional pressure drop is the same as that of the observed pressure drop. However, for trickle and spray flow regime, estimation of the fraction of liquid suspended in the gas phase (θ_L) is not straightforward. CFD-based models may be used to gain some insight into this.

In this study, we have investigated some of the aspects highlighted in this section using experimental and computational techniques. The experimental data as well as computational models discussed here will be useful for understanding and designing of trickle-bed reactors.

Experimental Setup and Operating Procedure

Trickle-bed reactors (perspex) of 0.114 and 0.194 m diameter and 1 m height were set up for experimental study. Stainless steel perforated (3 mm tringular pitch) was used for the top distributor and bottom support plate. Details of experimental setup and operating procedure are given by Gunjal et al.[26] and operating parameters considered in the present study are listed in Table 1. Wall pressure fluctuations were measured using a voltage output pressure transducer (having working capacity ±5 psi) (PCB Piezotronics Inc., USA, Model 106B50). These transducers were powered by ICP Battery power units (PCB Piezotronics Inc., USA, Model 480E06), which also act as amplifiers. The amplified

Table 1. Experimental Parameters and Operating Conditions in Present Study

	column A	column B
diameter, m	11.4×10^{-2}	19.4×10^{-2}
packing height, m	1	1
system	air−water	air−water
gas velocity, m/s	0.22−0.44	0.11−0.22
liquid mass flow rate, kg/m^{2}s	0 − 10	0 − 10
packing	spherical glass beads	spherical glass beads
packing diameter (d_p), m	3×10^{-3}, 6×10^{-3}	3×10^{-3}, 6×10^{-3}
porosity of bed, dimensionless		
$d_p = 3 \times 10^{-3}$, m	0.36	0.36
$d_p = 6 \times 10^{-3}$, m	0.37	0.37

signal was transferred to a microcomputer via a junction box. The analogue output of the ICP battery is first converted to a digital format using a 16-bit A/D PCMCIA converter card (nCode Inc. UK) and then stored into the microcomputer using dAtagate software (nCode Inc., UK). Wall pressure fluctuations were measured using a pressure transducer mounted at the middle (0.5 m) of the column (to minimize the end effects).

Before the start of each experiment, air was passed through the column at least for 5−6 h to ensure that complete dry bed conditions are achieved. For a nonwetted bed, the liquid flow rate was gradually increased and pressure drop and dynamic liquid holdup and wall pressure fluctuations were measured. Dynamic liquid holdup was measured by switching off the inlet air and liquid flows and by collecting the drained liquid. Acquired data were analyzed to examine the influence of sampling frequency, number of data points, and low pass filter frequency on the processed results. This analysis showed that the sampling frequency of 200 Hz and 2^{15} data points are adequate. Based on the preliminary analysis as well as results of Krieg et al.,[6] the low pass filter of 20 Hz was used for all the subsequent data processing.

Computational Model and Boundary Conditions

In trickle-bed reactors, catalyst pellets are usually packed randomly. The random packing of pellets of specific shape leads to nonuniform porosity distribution within the bed. Jiang[27] showed that appropriate representation of such a nonuniform porosity distribution in a CFD model is essential for qualitatively and quantitatively correct flow simulations. The details of implementation of nonuniform porosity and model equations are discussed below.

Representing Nonuniform Porosity Distribution. Numerous studies on porosity distribution in randomly packed beds are available (see, for example, Mantle et al.[28] and Stephenson and Stewart[29] for experimental study and Spedding and Spencer[30] for computational study). These experimental and computational studies have shown that the porosity is higher near the vicinity of the wall and it fluctuates significantly in the near wall region (of width of about 4 to 5 particle diameters). Mueller[31] has proposed a correlation for radial variation of axially averaged porosity as a function of column diameter, particle diameter, and average porosity. This correlation is fairly general and represents the available experimental data with reasonable accuracy. In the present work, we used this correlation (reproduced below as eq 2) to represent radial variation of axially averaged bed porosity.

$$\epsilon(r) = \epsilon_B + (1 - \epsilon_B) J_o(ar^*) e^{-br}$$

where

$$a = 8.243 - \frac{12.98}{(D/d_p - 3.156)} \quad \text{for } 2.61 \le D/d_p \le 13.0$$

$$a = 7.383 - \frac{2.932}{(D/d_p - 9.864)} \quad \text{for } 13.0 \le D/d_p \tag{2}$$

$$b = 0.304 - \frac{0.724}{D/d_p}$$

$r^* = r/D$ and J_0 is zeroth-order Bessel function

The predicted radial variation of bed porosity for 11.4 cm diameter is shown in Figure 2a.

Jiang[27] has shown that porosity variation in the axial direction (at any radial location) is close to Gaussian distribution. The value of standard deviation of such distribution decreases with an increase in the ratio of column diameter to particle diameter and eventually approaches zero for very small (compared to column diameter) particles. The porosity distribution within the randomly packed bed may thus be represented by imposing random fluctuations (following the Gaussian distribution) over the axially averaged porosity estimated by Mueller's correlation. 2d-axisymmetric computational domain was considered (see details in Figure 2b[A]). For generating such a distribution, the domain was divided into 25000 cells (50 in radial direction and 500 in axial direction). For cells located at the same radial location along the axial direction, porosity values were assigned by drawing a random number from the Gaussian distribution of specified standard deviation around the value obtained from Mueller's correlation. Simulated porosity distribution for a two-dimensional bed with a typical experimental configuration used for trickle-bed studies is shown in Figure 2b[B].

Model Equations. Several different approaches such as percolation theory approach (Crine et al.[32]), network model (Thomson and Fogler[33]), Eulerian−Eulerian approach with the multifluid models (Jiang,[27] Yin et al.,[34] Attou and Ferschneider,[35] and Grosser et al.[36]) and lattice Boltzmann-type models (Mantle et al.[28]) have been applied to simulate gas−liquid flow in packed beds. Grosser et al.[36] and Attou and Ferschneider[35] have used a one-dimensional flow model with uniform porosity distribution in the bed. The Eulerian−Eulerian approach with the two-dimensional multifluid models with spatial variation of the porosity appears to be most suitable for reactor engineering applications (Kashiwa et al.,[37] Jiang et al.,[24] and Ranade[38]) and was selected for the present work. In this approach, continuum approximation is applied for all the phases. Volume-averaged mass and momentum balance equations for

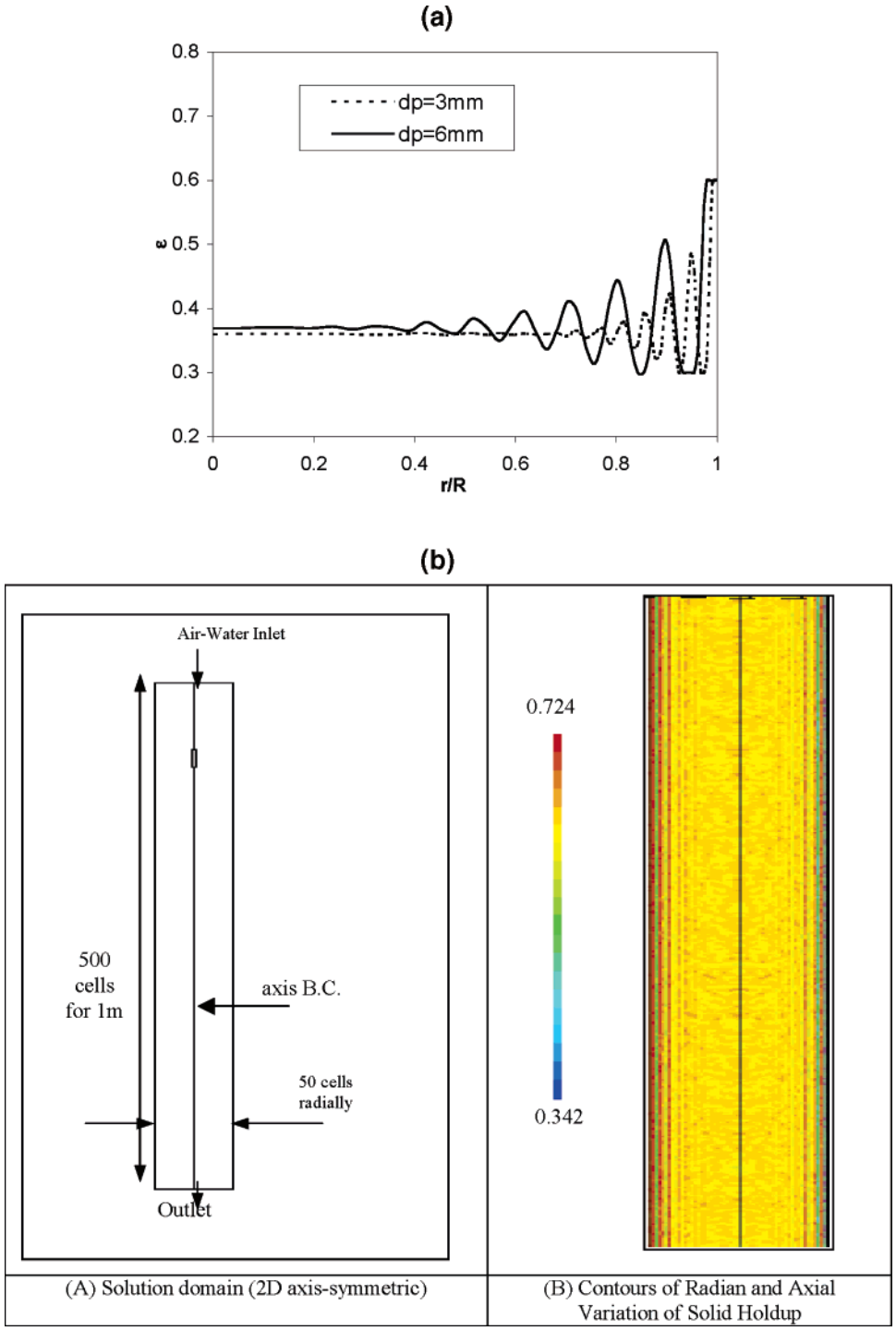

Figure 2. (a) Variation of the porosity along radial direction using Mueller[31] correlation for column diameter = 11.4 cm. (b) Bed model details and contours of simulated results (bed diameter 19.4 cm, d_p = 0.006 m, std dev = 5%).

the kth fluid can be written as

mass balance equation:

$$\frac{\partial \epsilon_k \rho_k}{\partial t} + \nabla \cdot \epsilon_k \rho_k U_k = 0 \qquad (3)$$

momentum balance equation:

$$\frac{\partial(\epsilon_k \rho_k U_k)}{\partial t} + \nabla \cdot (\epsilon_k \rho_k U_k U_k) = -\epsilon_k \nabla P_k + \nabla \cdot (\epsilon_k \mu \nabla U) + \epsilon_k \rho_k g + F_{k,R}(U_k - U_R) \qquad (4)$$

where ϵ_k represents the volume fraction of each phase, ρ_k is the density of the kth phase, U_k is the cell velocity of the kth phase, P is a mean pressure shared by all the phases present in the system, and $F_{k,R}$ is the interphase momentum exchange terms. The left-hand side of eq 4 represents the rate of change of momentum for the kth phase. The right-hand side represents pressure forces, gravitational acceleration, average shear stresses, and interphase momentum exchange. In the present work, the gas phase was treated as a primary phase and liquid−solid phases were treated as secondary phases. The solid phase was considered as

stationary and distribution of the solid volume fraction was assigned at the beginning of the simulation, which remains invariant throughout the simulation.

The pressure drop in the packed bed is usually correlated using the Ergun equation or its variants (Al-Dahhan et al.,[10] Holub et al.,[39] and Saez and Carbonell[11]). Interphase coupling terms may therefore be formulated based on similar equations. The presence of liquid flow, however, leads to additional interphase exchanges, which need to be formulated correctly. Different approaches, viz, relative permeability model (Saez and Carbonell[11] and Grosser et al.[36]), slit model (Holub et al.[40]), and two-fluid interaction model (Attou and Ferschneider[22] and Attou and Ferschneider[35]) have been proposed to formulate interphase momentum exchange terms. We have used the model of Attou and Ferschneider,[35] which includes gas−liquid interaction force and has a more theoretically sound basis. The model of Attou and Ferschneider[35] was developed for the regime in which liquid flows in the form of film. In this work, we have explored the possibility of using this model for simulating flow regimes in which part of the liquid may flow in the form of droplets. The interphase coupling terms $F_{k,R}$ (given here by eqs 4−7) proposed by Attou and Ferschneider[22] are rewritten in terms of interstitial velocities and phase volume fractions as (instead of superficial velocities and saturation)

gas−liquid momentum exchange term:

$$F_{GL} = \epsilon_G\left(\frac{E_1\mu_G(1-\epsilon_G)^2}{\epsilon_G^2 d_p^2}\left[\frac{\epsilon_S}{(1-\epsilon_G)}\right]^{0.667} + \frac{E_2\rho_G(U_G-U_L)(1-\epsilon_G)}{\epsilon_G d_p}\left[\frac{\epsilon_S}{(1-\epsilon_G)}\right]^{0.333}\right) \quad (5)$$

gas−solid momentum exchange term:

$$F_{GS} = \epsilon_G\left(\frac{E_1\mu_G(1-\epsilon_G)^2}{\epsilon_G^2 d_p^2}\left[\frac{\epsilon_S}{(1-\epsilon_G)}\right]^{0.667} + \frac{E_2\rho_G U_G(1-\epsilon_G)}{\epsilon_G d_p}\left[\frac{\epsilon_S}{(1-\epsilon_G)}\right]^{0.333}\right) \quad (6)$$

liquid−solid momentum exchange term:

$$F_{LS} = \epsilon_L\left(\frac{E_1\mu_L\epsilon_S^2}{\epsilon_L^2 d_p^2} + \frac{E_2\rho_L U_G\epsilon_S}{\epsilon_L d_p}\right) \quad (7)$$

It must be noted that a pressure shared by all the phases is used in the momentum balance equation (eq 4). However, when two immiscible phases are in contact with each other, interfacial tension causes the fluids to have different pressures. Such a pressure difference (capillary pressure) for the gas and liquid phase may be written as

$$P_G - P_L = 2\sigma\left(\frac{1}{d_1} - \frac{1}{d_2}\right) \quad (8)$$

where d_1 and d_2 are the maximum and minimum diameter of the sphere with liquid film formed by the flowing liquid. More details of relating d_1 and d_2 to particle diameter, porosity, and the minimum equivalent diameter of the area between three particles in contact are given in Attou and Ferschneider.[22] Capillary pressure affects the liquid distribution and may set up gradients of liquid holdup within the packed bed.

Several investigators have analyzed capillary forces (for example, Grosser et al.,[36] Attou and Ferschneider,[22] Jiang et al.,[23] and references therein). Grosser et al.[36] have studied the onset of pulsing in trickle beds using linear stability analysis. Their analysis suggests that the competition between the inertial and capillary forces leads to a situation in which steady-state flow is not possible, implying the pulsing in trickle beds. In the present work, the pulsing regime was not considered and the scope was restricted to trickle and spray flow regimes. Grosser et al.[36] have proposed the capillary pressure as an empirical function of the liquid saturation:

$$P_L = P_G - \sigma\frac{\epsilon_S E_1^{0.5}}{(1-\epsilon_S)d_p}[0.48 + 0.036\ln(1-\beta_L)/\beta_L] \quad (9)$$

The order of magnitude analysis indicates that the magnitude of the capillary forces is rather small compared to the magnitudes of interphase drag forces. Attou and Ferschneider[22] have obtained the following expression for the capillary pressure term based on geometric estimates of d_1 and d_2 and with empirical factor F to account for high-pressure operations as

$$P_G - P_L = 2\sigma\left(\frac{1-\epsilon}{1-\epsilon_G}\right)^{0.333}\left(\frac{5.416}{d_p}\right)F\left(\frac{\rho_G}{\rho_L}\right) \quad (10)$$

where

$$F\left(\frac{\rho_G}{\rho_L}\right) = 1 + 88.1\frac{\rho_G}{\rho_L} \quad \text{for } \frac{\rho_G}{\rho_L} < 0.025 \quad (11)$$

Under typical operating conditions of trickle beds, quantitative comparison of the capillary pressures estimated from eq 9 and eq 10 are not very different (within 10%). Considering the geometric basis used by Attou and Ferschneider,[22] eq 10 was incorporated into the present CFD model.

The pressure drop required to maintain specified gas and liquid throughputs is history dependent. Pressure drop at any specific liquid velocity measured with increasing liquid velocity is more than that measured with decreasing liquid velocity (see, for example, Szady and Sundaresan[41]). Capillary phenomenon is one of the contributing factors of this observation. Jiang et al.[23] have attempted to simulate this phenomenon by introducing an empirical factor (f) related to the degree of wetting in their capillary pressure formulation as

$$P_G - P_L = (1-f)P_c \quad (12)$$

For a prewetted or fully wetted bed, f was set to 1, implying zero capillary pressure. For a nonwetted bed, f was set to zero (Jiang et al.[23]). For incorporating the capillary pressure in the CFD model, gradients of capillary pressure must be formulated as

$$\frac{\partial P_G}{\partial z} - \frac{\partial P_L}{\partial z} = \frac{2}{3}\sigma\frac{5.416}{d_p}\left(\frac{\epsilon_S}{1-\epsilon_G}\right)^{-2/3}\left(\left(\frac{1}{1-\epsilon_G}\right)\frac{\partial\epsilon_S}{\partial z} + \left(\frac{\epsilon_S}{(1-\epsilon_G)^2}\right)\frac{\partial\epsilon_G}{\partial z}\right)F\left(\frac{\rho_G}{\rho_L}\right) \quad (13)$$

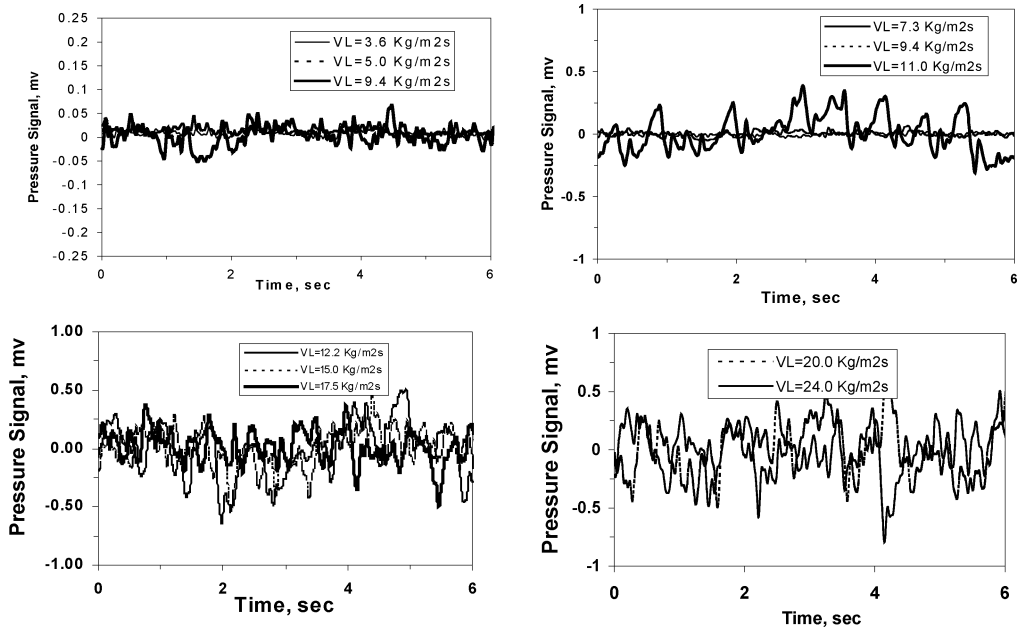

Figure 3. Wall pressure fluctuations in TBR at various liquid flow rates (V_G = 0.22 m/s).

Equation 13 was used to express the gradients of liquid pressure (P_L) in the liquid-phase momentum equations in terms of gradients of gas pressure (P_G) to incorporate the capillary pressure terms.

Boundary Conditions and Numerical Solution. A two-dimensional axis symmetric domain was considered (see Figure 2b[A]). The above set of model equations was implemented in commercial software FLUENT 6.1 (of Fluent. Inc., USA) using user-defined routines. Porosity for each cell was assigned via A user-defined subroutine and the velocity of the solid phase was set to zero. A flat velocity profile was implemented for gas and liquid phases as an inlet boundary condition. To minimize the discontinuity at the inlet, we estimated the overall liquid volume fraction, $\langle \epsilon_L \rangle$, using the available correlations and used it to specify inlet boundary conditions as

$$U_{Lin} = \frac{(V_L/\rho_L)}{\langle \epsilon_L \rangle} \qquad U_{Gin} = \frac{(V_G/\rho_G)}{1 - \langle \epsilon_L \rangle} \tag{14}$$

where V_L and V_G are the mass fluxes of liquid and gas, respectively (kg/m^{2}s), and ρ_L and ρ_G are the densities of liquid and gas, respectively.

No slip boundary condition was used for all the impermeable walls. Momentum exchange between the phases was set in the model using user-defined subroutines. Unsteady simulation was carried out with a time step of 0.005 s. Preliminary numerical experiments were carried out to identify the computational cells are adequate to obtain grid independent results. These numerical experiments indicated that the predicted values of overall pressure drop and liquid saturation become insensitive to further grid refinement (4 times increase in the number of grid cells and use of higher order discretization scheme caused less than 5% change in pressure drop and less than 0.75% change in liquid volume fraction).

Results and Discussion

Dynamics of Gas−Liquid Flows and Regime Transition. Wall pressure fluctuations were measured for various liquid flow rates at constant gas velocity (0.22 m/s). Typical wall pressure fluctuations data at various liquid flow rates is shown (after low pass filtering) in Figure 3. In a trickle flow regime, weak fluctuations in the pressure signal were observed (Figure 3a). Amplitude of pressure fluctuations increases as one moves from trickle to pulse flow regime (Figure 3b). The pulsing was observed at a liquid flow rate above 11 kg/m^{2}s (Figure 3b). The pulsing observed at this liquid flow rate was uniform in nature. The nature of pulsing remained relatively uniform up to the liquid velocity of 15 kg/m^{2}s (Figure 3c). Nonuniformity of pulsing started with a further increase in liquid flow rate (17.4 kg/m^{2}s). Beyond this point, further increase in liquid flow rate (20 kg/m^{2}s), gas−liquid dispersed flow was observed. In this operating regime, pressure signals were highly nonuniform (Figure 3d).

Power spectra of acquired wall pressure fluctuations data at different liquid flow rates are shown in Figure 4. For single-phase flow, the figure shows a dominant peak at low frequency (<0.5), which is inherent in the system. This frequency remained dominant at all liquid flow rates. In the trickle flow regime (up to 7 kg/m^{2}s) other frequencies were absent. For liquid flow rates higher than 7 kg/m^{2}s, peaks at frequencies higher than 1 Hz appear in the power spectrum. Between liquid flow rates of 9.4 and 11 kg/m^{2}s, transition from trickle to pulse flow regime was observed and a distinct peak of frequency 1.85 Hz was observed at liquid flow rate 11 kg/m^{2}s (Figure 4b). At higher liquid flow rate (above 15 kg/m^{2}s), more peaks appear in the power spectrum (Figure 4c). Generally, the key characteristic frequency was within the range of 1−2 Hz with some smaller peaks around 3−4.0 Hz (Figure 4d). At higher liquid flow rates (dispersed bubble pulse flow regime, Figure 4d), the spectrum becomes wider, indicating a large number of temporal scales interacting with each other.

There are a number of ways one can use to obtain information about key dynamic characteristics from the acquired time series. Here we have characterized the dynamics of trickle beds using the Kolmogorov entropy. The wall pressure fluctuations data were processed

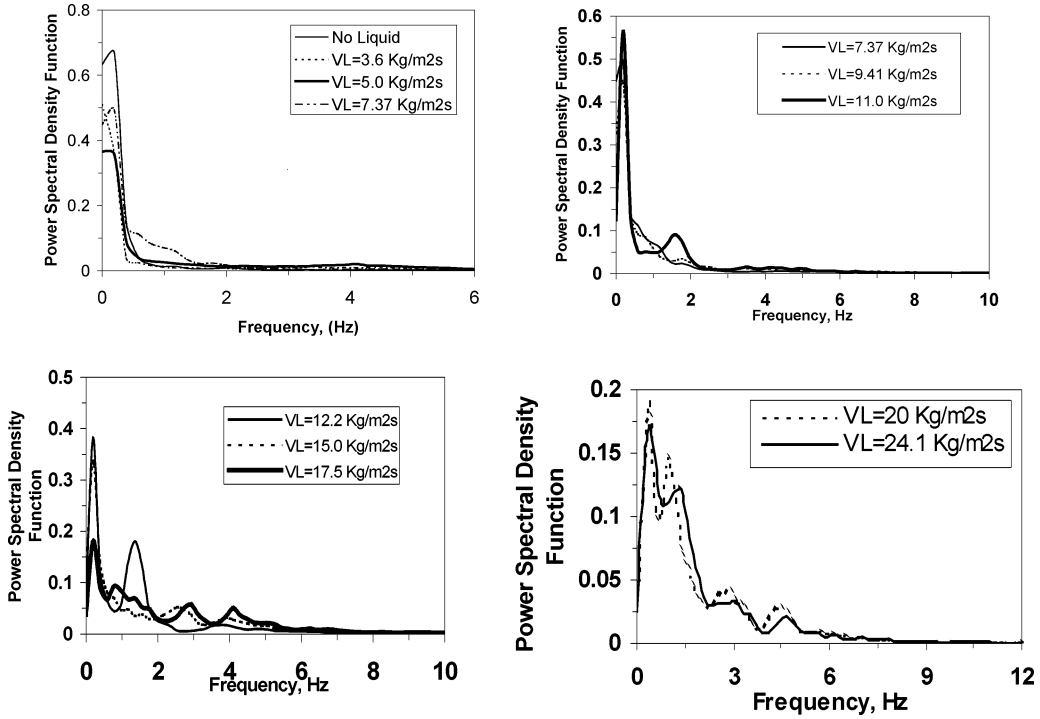

Figure 4. Power spectral density at various liquid flow rates (V_G = 0.22 m/s).

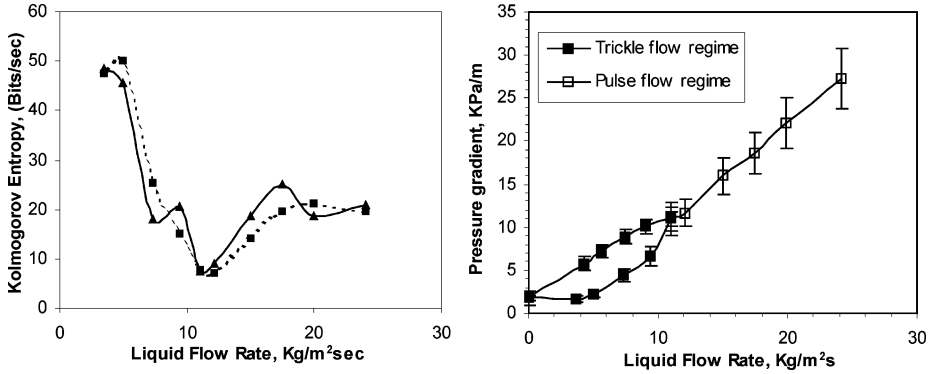

Figure 5. Trickle to pulse flow regime transition: Kolmgorov entropy and pressure drop hysteresis (D = 0.114 m, d_p = 3 mm, and V_G = 0.22 m/s).

using AnTS (nonlinear **An**alysis of **T**ime **S**eries, see Ranade and Utikar[42] for more details) with a low pass frequency of 20 Hz. The Kolmogorov entropy represents the rate of information loss of the system. Following Schouten et al.,[43] the maximum likelihood estimate of Kolmogorov entropy was obtained using 2^{15} data points (32768 data points sampled with a frequency of 200 Hz). The cutoff length was set equal to the average absolute deviation of the entire time series and the delay time was chosen equal to the sample interval time. The entropy values were calculated with embedding dimension set to the average number of points per cycle (see Ranade and Utikar,[41] for a detailed discussion). The variation of the Kolmogorov entropy with liquid flow rate is shown in Figure 5a. The value of Kolmogorov entropy decreases continuously with liquid flow rate until it reaches a value of 11 kg/m^{2}s (from 50 to 7 bits/s). The lowest value of the Kolmogorov entropy was found to coincide with the transition from trickle to pulse flow regime. It can be seen from Figure 5a that variation of Kolmogorov entropy indicates a sharp transition from trickle to pulse flow regime. It should be noted that the transition from trickle to pulse flow regime may not always be that sharp. At higher liquid velocity (above 11 kg/m^{2}s), in the pulse flow regime, the Kolmogorov entropy increases with an increase in liquid flow. In a dispersed bubble pulse flow regime (above 20 kg/m^{2}s), the Kolmogorov entropy remained more or less constant. It can be seen that variation of Kolmogorov entropy can be conveniently used to accurately identify regime transition from trickle to pulse flow regimes.

Time-Averaged Pressure Drop and Liquid Holdup. Two-phase pressure drop per unit length and dynamic liquid holdup at different liquid flow rates for prewetted and non-prewetted bed conditions were measured. To estimate the total liquid holdup in the bed, the static liquid holdup was calculated from the correlation of Saez and Carbonell[10] and was added to the measured dynamic liquid holdup. Static holdup is a function of Eotvos number ($\ddot{E}$), contact angle at the gas−liquid contact line, and geometry of packing and was calculated as follows,

$$\epsilon_{SL} = \frac{1}{20 + 0.9\ddot{E}} \tag{15}$$

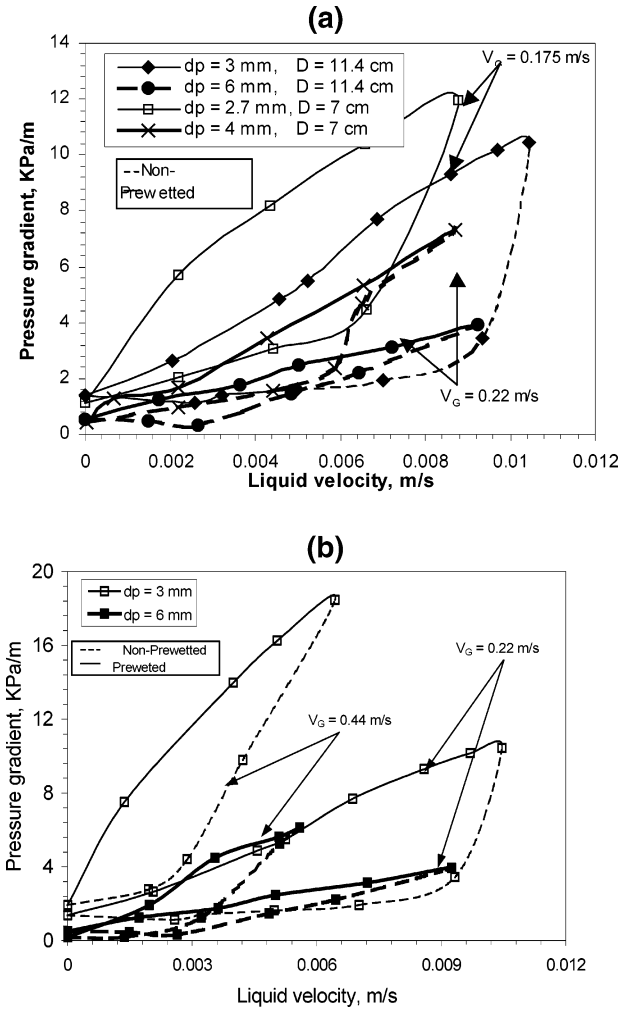

Figure 6. (a) Pressure drop and liquid hold-up hysteresis in TBR at various operating conditions (data of $D = 7$ cm from Wang et al.[44]). (b) Pressure drop and liquid hold-up hysteresis in TBR at various operating conditions for $D = 11.4$ cm.

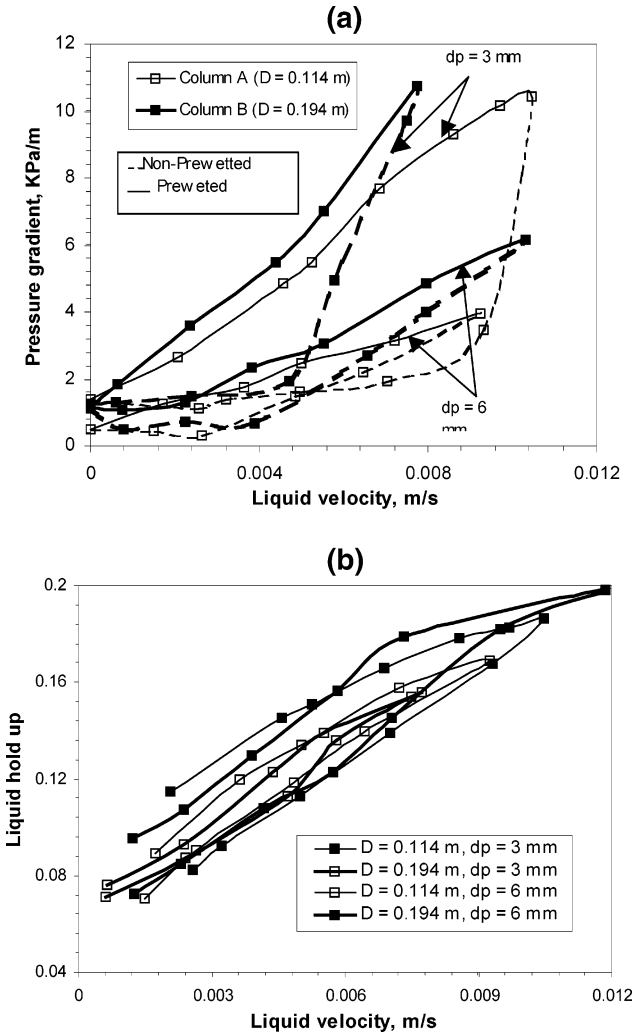

Figure 7. (a) Effect of column diameter on pressure drop hysteresis at $V_G = 0.22$ m/s. (b) Liquid holdup in different trickle-bed reactors at $V_G = 0.22$ m/s.

where

$$\ddot{E} = \frac{\rho_L g d_p{}^2 \epsilon^2}{\sigma_L (1 - \epsilon^2)^2} \tag{16}$$

where ρ_L and σ_L is the density and surface tension of the liquid phase. At all gas velocities static holdup for 3 mm and 6 mm particles was 0.049 and 0.048, respectively.

Typical time-averaged pressure drop data at various liquid velocities is shown in Figure 6b. It can be seen that the pressure drop variation with liquid flow rate shows two branches: the lower bench is for the non-prewetted bed (increasing liquid flow rate mode) while the upper bench shows data for the pre-wetted bed (decreasing liquid flow rate mode). When the liquid flow rate was slowly increased from zero in a dry bed, the lower branch was obtained. The bed becomes completely wet just before transition to a pulse flow regime occurs. When the liquid flow rate was decreased slowly back to zero from the higher liquid velocity, pressure drop variation showed hysteresis and followed an upper branch. For a dry bed, the capillary pressure acting on the solid−liquid contact line is dominant, which restricts the spreading within the bed. Thus the liquid flows through the confined region of the bed. This pattern gets disrupted at the flow transition point. When the liquid flow rate was decreased, due to radial spreading and vigorous mixing earlier, there is a larger amount of gas−liquid interfacial interaction, which results in higher pressure drop along the upper branch. The pressure difference between the upper and lower branch may vary considerably depending on the extent of prewetting and intermediate values can be obtained through various inner loops. Similar trends of hysteresis were observed for liquid holdup in the bed as well.

Influence of particle size on pressure drop hysteresis is shown in Figure 6a. It can be seen that the magnitude of hysteresis decreases with an increase in particle diameter. Similar results were reported by Wang et al.[44] whose data is also shown in Figure 6a. As the particle diameter increases, characteristic dimension of interstitial space also increases. Therefore, capillary pressure becomes less dominant. Overall pressure drop also decreases with increase in particle diameter. Therefore, magnitude of pressure drop hysteresis decreases with increase in particle size. The effect of gas velocity on hysteresis loop is shown in Figure 6b. It can be seen that the magnitude of hysteresis in pressure drop is not very sensitive to the gas velocity. At higher gas velocity, transition of the pulse flow regime occurs at lower liquid velocity.

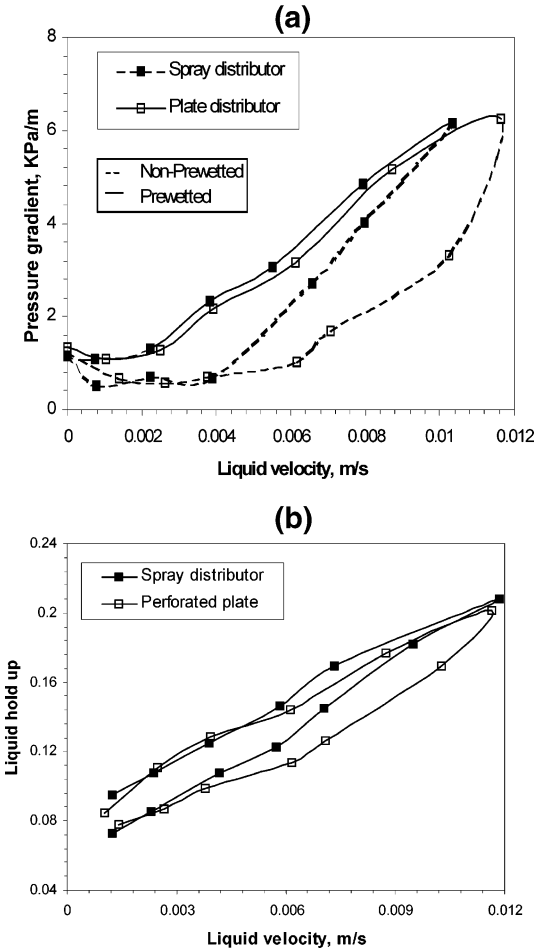

Figure 8. (a) Effect of liquid inlet distributor on pressure drop hysteresis (V_G = 0.22 m/s, d_p = 6 mm, D = 0.194). (b) Liquid holdup for different distributors (V_G = 0.22 m/s, d_p = 6 mm, D = 0.194 m).

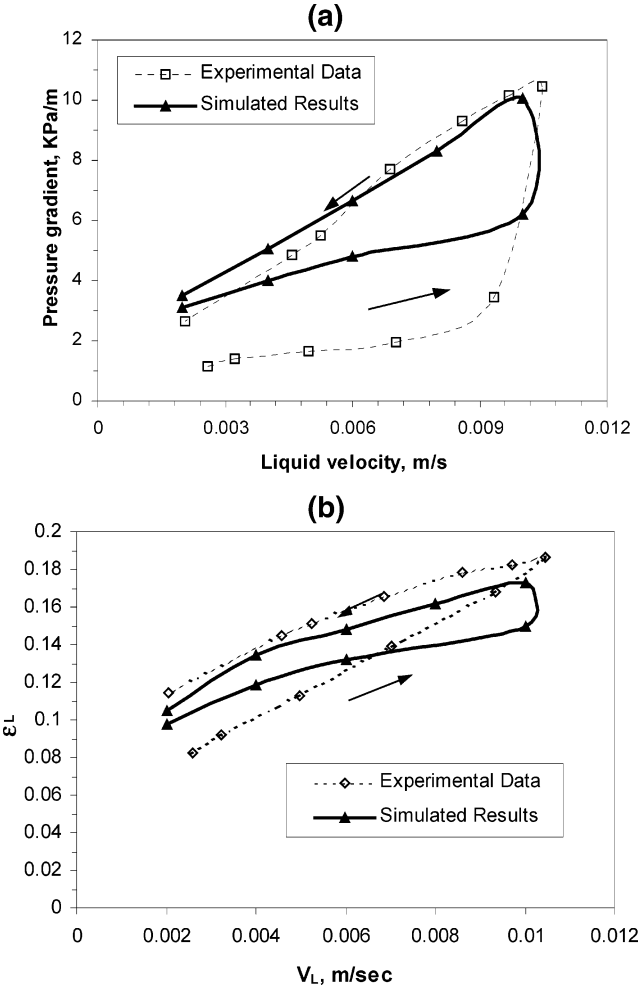

Figure 9. (a) Comparison of simulated results of pressure drop for prewetted and non-prewetted beds (V_G = 0.22 m/s, std dev = 5%, D = 0.114 m, d_p = 3 mm). (b) Comparison of simulated results of liquid holdup for prewetted and non-prewetted beds (V_G = 0.22 m/s, std dev = 5%, D = 0.114 m, d_p = 3 mm).

With increase in column diameter, the observed pressure drop was found to increase slightly (see Figure 7). The variation of total liquid holdup as a function of liquid velocity for two column diameters is shown in Figure 7b. It can be seen that there is no significant change in the observed liquid holdup with bed diameter. Since hysteresis behavior depends on initial flow distribution in the bed, experiments were carried out with two types of liquid distributors (spray and a perforated plate). The magnitude of pressure drop hysteresis observed with the spray distributor was smaller than that for the perforated plate distributor (Figure 8a). Visual inspection also confirmed that the spray distributor was able to realize better liquid distribution within the bed. Similar results were also observed for the hysteresis in liquid holdup (Figure 8b). The data collected in this work will be useful for evaluating computational models.

Comparison of Model Predictions with Experimental Data. Predictions of the CFD model discussed in the previous section were first compared with our experimental data in a trickle flow regime for 0.114 m and 0.194 m column diameter (see details in Table 1). Effect of prewetted and non-prewetted bed conditions was considered in the model. The validated model was then used to simulate some of the published experimental data covering a wide range of operating conditions (see Table 2). For this purpose three different data sets (from Szady and Sundaresan,[41] Rao et al.,[45] and Spacchia and Baldi[46]) were selected. The CFD model was then used to estimate the extent of suspended liquid in a trickle flow regime and to simulate periodic operation of trickle beds to obtain insight into a pulse flow regime.

Table 2. Details of Bed Characteristics and Operation Conditions Used in Simulations

case	data source	D/d_p	bed characteristics	V_G, (m/s)	$V_L \times 10^3$ (m/s)	Ergun's constant used for simulations E_1 & E_2
1	Szady and Sunderesan[41]	55	3 mm spherical e_B = 0.37	0.22	0.2−0.8	215 & 1.75
2	Specchia and Baldi[46]	29.6	2.7 mm spherical e_B = 0.38	0.2−0.8	2.8	500 & 3
3	Rao et. al[45]	15.4	3 mm spherical e_B = 0.37	1.5−5.5	1.0	215 & 3.4

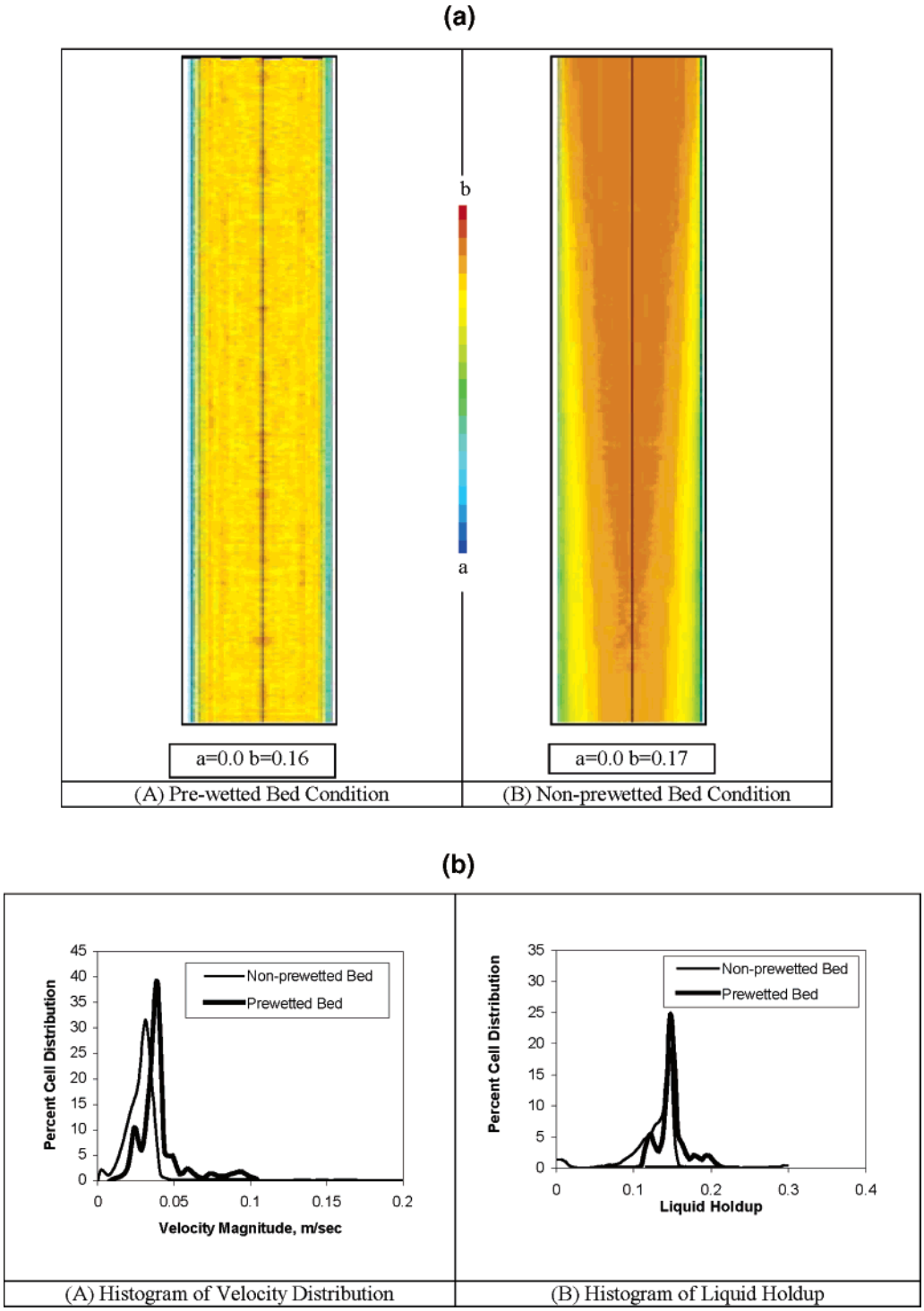

Figure 10. (a) Simulated contours of liquid holdup for prewetted and non-prewetted beds (V_L = 6 kg/m^{2}s, V_G = 0.22 m/s, std dev = 5%, D = 0.114 m, d_p = 3 mm). (b) Histogram of simulated results of liquid velocity and holdup (V_L = 6 kg/m^{2}s, V_G = 0.22 m/s, std dev = 5%, D = 0.114 m, d_p = 3 mm).

Observed hysteresis in pressure drop is associated with the capillary pressure. Accurate representation of capillary terms in the CFD model is difficult. In this work, we have used the capillary pressure model developed by Attou and Ferschneider.[22] The simulations were carried out by setting the value of "*f*" to 1 for prewetted beds and to zero for a dry bed and results were compared with the experimental data in Figures 9a and 9b. As observed in the experiments, simulated results showed lower pressure drop for the dry bed compared to the prewetted bed. The predicted magnitude of the hysteresis is however lower than that observed in the experiments. For the dry bed (lower branch as well as the initial part of the upper branch), experimental data showed nonlinear variation of pressure drop with liquid velocity. However, simulated results showed almost a linear variation. The inadequate representation of capillary forces is the most likely cause of this discrepancy. Nonlinearity appears even in the upper branch mainly because when liquid velocity is reduced, partial dry-out may occur in the bed, making it similar to the non-prewetted bed. Simulated contours of liquid holdup for a prewetted bed and non-prewetted bed are shown in Figure 10a. Liquid distribu-

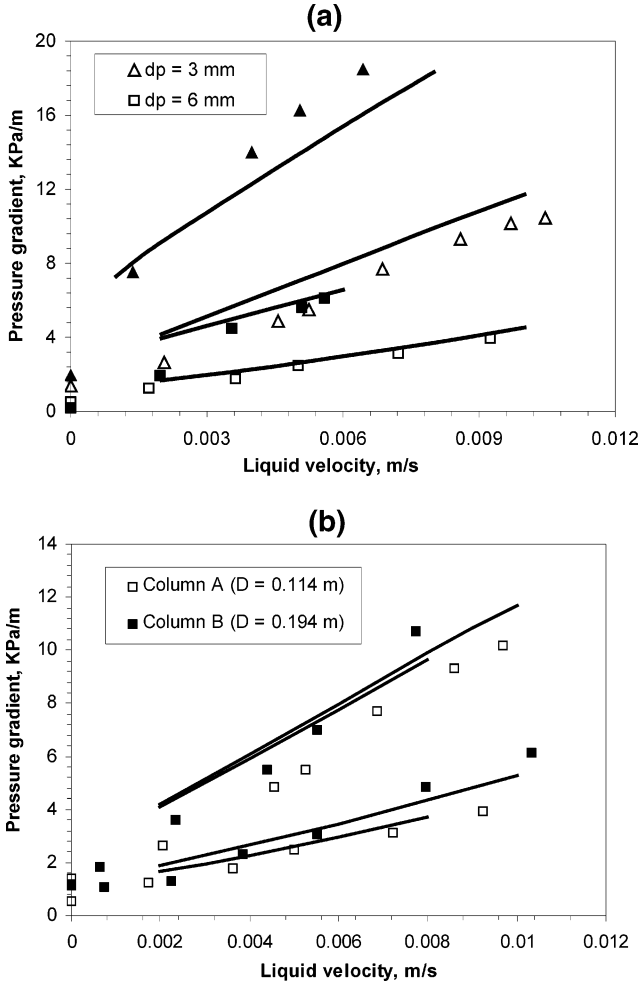

Figure 11. (a) Comparison of CFD results with experimental data for $D = 0.114$ m (filled symbols: $V_G = 0.44$ m/s; unfilled symbols: $V_G = 0.22$ m/s). (b) Comparison of CFD results with experimental data with $d_p = 3$ mm (filled symbols: $V_G = 0.44$ m/s; unfilled symbols: $V_G = 0.22$ m/s).

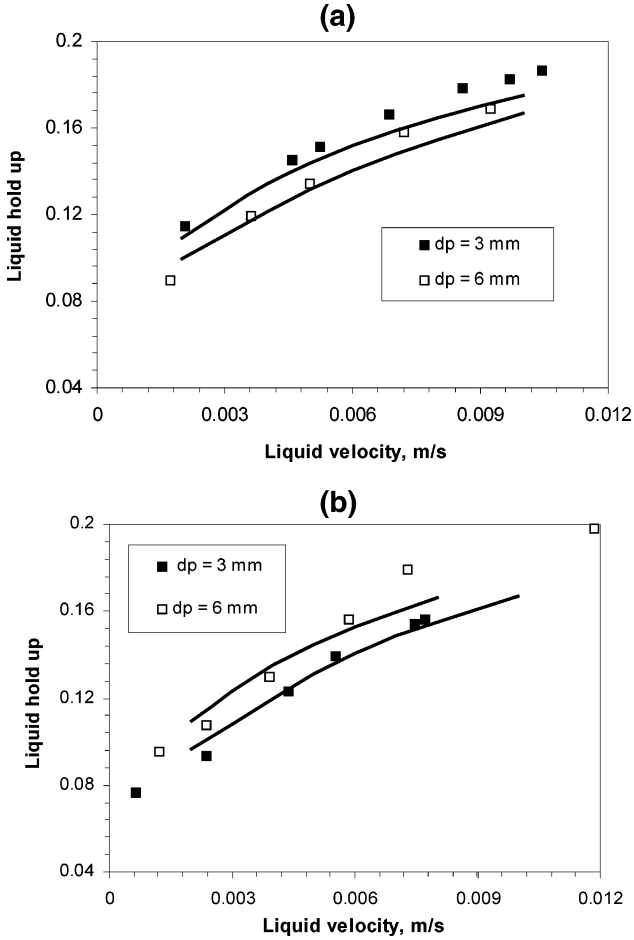

Figure 12. (a) Comparison of CFD results with experimental data ($D = 0.114$ m, $V_G = 0.22$ m/s). (b) Comparison of CFD results with experimental data ($D = 0.194$ m, $V_G = 0.22$ m/s).

tion in a prewetted bed is relatively uniform as compared to the non-prewetted bed conditions (Figure 10a(A)). It can be seen from Figure 10b that velocity and hold-up distributions within the bed for the liquid phase for pre- and non-prewetted beds are substantially different. Distributions for the prewetted bed are wider than those for a non-prewetted bed.

For a prewetted bed, simulated results of pressure drop for the 0.114 m diameter of a column are compared with the experimental data (Figure 11a) for gas velocities 0.22 m/s and 0.44 m/s. Simulated results overpredict pressure drop for a 3 mm particle ($E_1 = 215$, $E_2 = 1.8$) at low gas velocity (0.22 m/s) and underpredict for high gas velocity ($V_G = 0.44$ m/s). However, for 6 mm particles ($E_1 = 500$, $E_2 = 2.4$), simulated results show reasonable agreement with the experimental data. While interpreting the observed differences in the predicted and experimental results for two particle sizes, it should be noted that magnitude of hysteresis is much larger for the smaller particle. In such a case, the exact locations of upper and lower branch (of pressure drop versus liquid velocity) depend on the degree of wetting. Such sensitivity to the degree of wetting may be one of the reasons for the observed discrepancy. For the larger particle, where magnitude of hysteresis is lower, influence of such sensitivity is much less. Another possible reason behind the observed discrepancies might be uncertainty associated with the axial variation of porosity (dependence of variance on particle size). The disagreement at low liquid velocity for $V_G = 0.44$ m/s may be due to a dry-out phenomenon at high gas flow rate. Influence of column diameter on agreement between simulated and experimental data is shown in Figure 11b. Simulated results show reasonably good qualitative as well as quantitative agreement with experimental data for 0.114 m and 0.194 m columns (see Figures 12a and 12b).

Extending CFD Models To Estimate the Fraction of Suspended Liquid. To cover the wider range of operating conditions, three independent experimental data sets were selected for evaluating the computational model. Details of bed characteristics and operation conditions used in these three cases are summarized in Table 2. In Case 1, the column to particle diameter (D/d_p) ratio was much higher compared to that of the other two cases. In Case 1 variation of pressure drop and liquid saturation was studied with change in liquid mass flow rate, while the effect of change in the gas mass flow rate on hydrodynamic parameters was studied in the other two cases. Gas mass flow rate in Case 3 was much higher than the other two cases.

Simulated results were compared with the experimental data of Szady and Sundaresan[41] for pressure drop and total liquid saturation in Figures 13a (only upper branch of pressure drop curve is shown here). The values of Ergun's (E_1 and E_2) constants used in the closure models represent the bed-packing characteris-

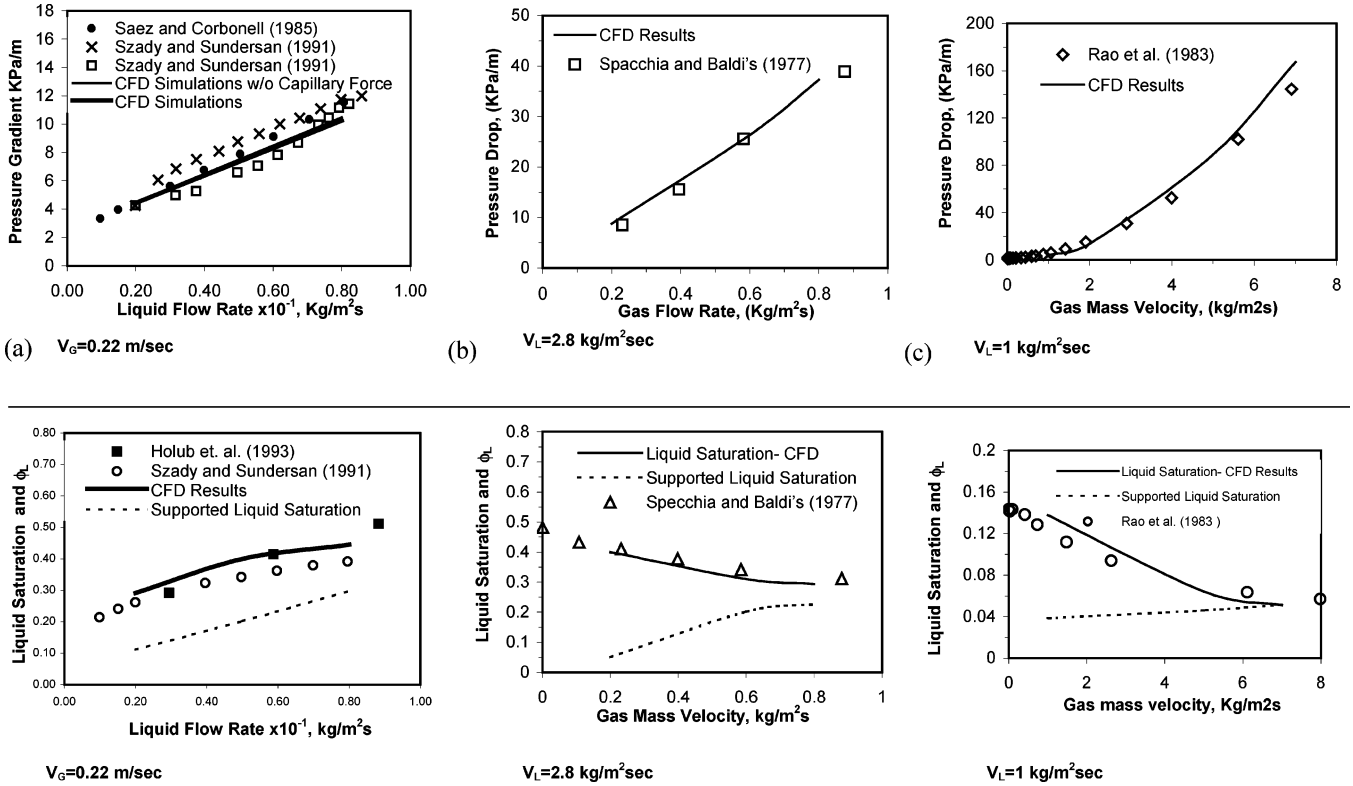

Figure 13. Comparison of simulated pressure drop and liquid saturation with literature data.

tics. In this case, $E_1 = 215$ and $E_2 = 1.75$ were used for carrying out the simulations. At low liquid velocities, the model showed good agreement with the experimental data. At higher liquid velocities (~8 kg/m^{2}s), the model underpredicted the pressure drop values. This may be because of the possible transition from trickle flow to pulse flow regime. Model predictions for pressure drop and liquid saturation for experimental data of Spacchio and Baldi[46] is shown in Figure 13b. In this case, higher values of Ergun's constants ($E_1 = 500$ and $E_2 = 3$) were used in the model. These values are close to the values suggested by Holub et al.[40] In this case, model predictions showed good agreement with the experimental data of pressure drop and liquid saturation. A third set of data from Rao et al.,[45] which was obtained for very high gas velocities compared to earlier data sets (1−8 kg/m^{2}s) was also used for evaluating the model predictions. As the velocity of the gas phase increases (>1.5 kg/m^{2}s), the trickle flow regime may change to a spray flow regime. It can be seen from Figure 13c that the model predictions showed good agreement with the experimental data for the high gas velocity cases as well (with $E_1 = 215$ and $E_2 = 3.4$). Though the value of E_2 looks rather high, it is well within the range of values used by previous investigators (see a review given by Holub et al.[39]).

Encouraged by such agreement, the CFD model developed here was used to estimate frictional pressure drop and supported liquid saturation. For this purpose, simulations were carried out for two values of gravitational acceleration. The detailed procedure for calculation of frictional pressure drop and supported liquid holdup is discussed in the Appendix. Following this procedure, frictional pressure drop and liquid saturation supported by the gas phase were calculated. The predicted values of supported liquid saturation are shown by a dotted line in Figure 13a−13c. It can be seen from Figure 13a that the fraction of liquid supported by the gas phase increases with liquid velocity. The results shown in Figures 13b and 13c indicate that the fraction of supported liquid saturation increases with gas velocity though the increase in gas velocity decreases the total liquid holdup or saturation. At very high gas velocity (see Figure 13c) almost all the liquid holdup is supported by the gas phase, indicating the spray flow regime. Thus the procedure discussed in the Appendix can be used to estimate the fraction of liquid supported by the gas phase and to identify possible transition to a spray regime.

CFD Simulations of Periodic Flow. In many industrial practices, liquid-induced periodic operations are preferable because reactor operation with natural pulsing is difficult for large reactors. It is worthwhile to apply present CFD model to simulate periodic operation of a trickle bed. This will also help to gain an insight into features of the pulse flow regime. In natural pulse flow regime, liquid-enriched pulses form after some distance from the inlet and they accelerate while moving downward. Formation of pulses is associated with complex interactions among capillary forces, wall adhesion, and the convective forces. If the model equations adequately represent this underlying physics and numerical solution does not add any artificial diffusivity, the simulated results should be able to capture the transition from trickle to pulse flow regime. However, the current understanding of physics of pulse formation and its implementation in the CFD model is not adequate for this purpose. An alternative way to gain some insight into pulse-like flow in trickle beds is to simulate periodic operation of trickle beds with induced pulses by manipulating inlet liquid velocity. Boelhouwer et al.[47] have compared the key features of natural pulsing and induced pulsing trickle beds. Their results showed that the variation between natural pulsing and induced pulsing is within 25%. Following this, we have simulated flow in trickle beds operated with liquid-

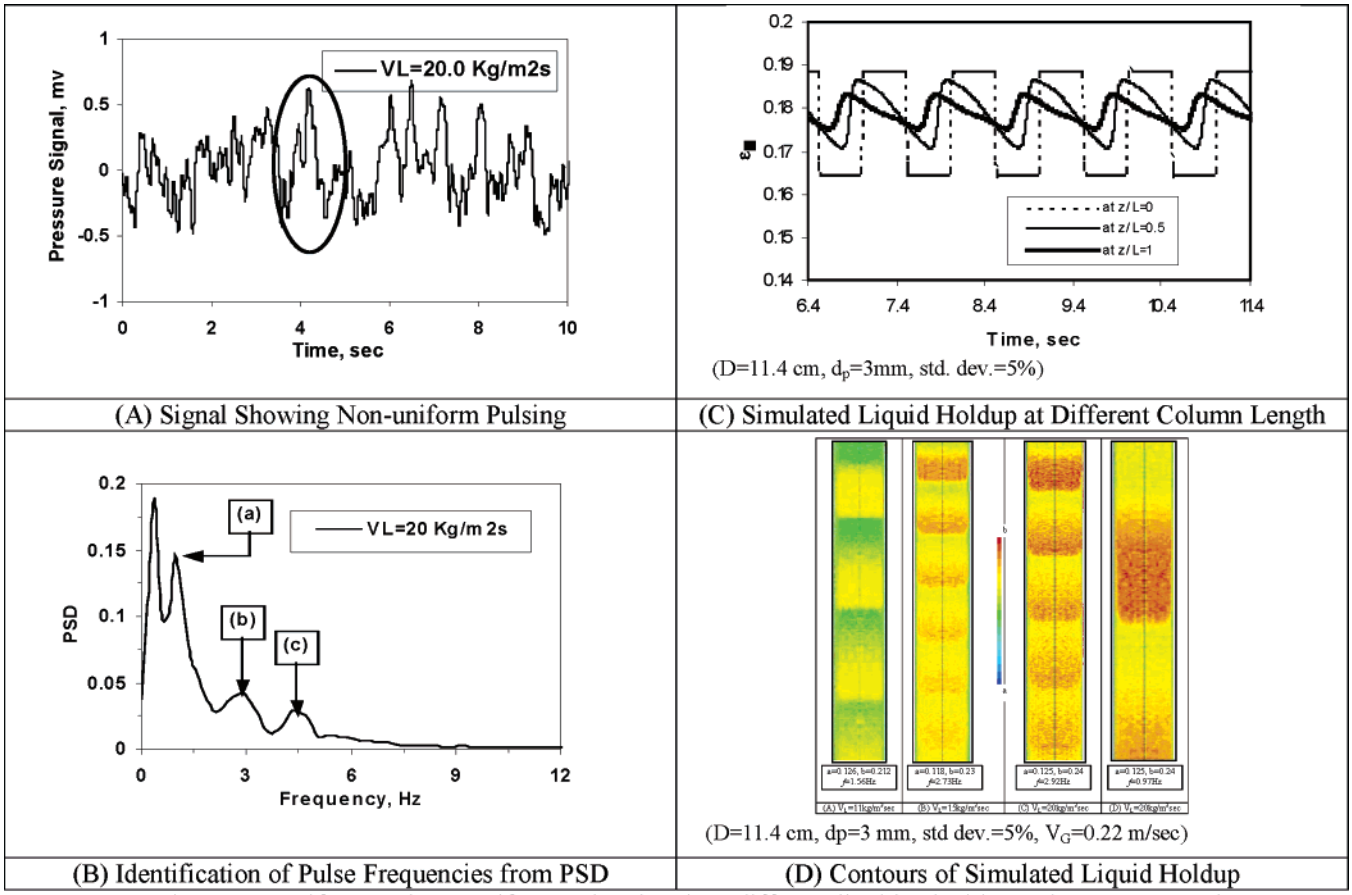

Figure 14. Uniform and nonuniform pulse signals at different liquid velocities and at $V_G = 0.22$ m/s.

Table 3. Frequencies of Different Pulses Obtained from PSD at $V_G = 0.22$ m/s

liquid flow rate kg/m^{2}s	a, s^{-1}	b, s^{-1}	c, s^{-1}
11.0	**1.562**		
12.2	**1.367**	3.7	
15	**2.73**	3.9	
17.5	0.78	**2.92**	4.1
20	**0.97**	**2.92**	4.49
24	1.36	**3.125**	4.68

induced pulsing, maintaining the same average flow rates. The frequency of liquid-induced pulsing was set from the experimental measurements of natural pulsing.

As discussed earlier, at low liquid flow rates (~11−12 kg/m^{2}s), pulse frequencies are quite uniform (see pressure signal in Figure 3 and a single peak in PSD at 1.56 Hz shown in Figure 4). At higher liquid flow rates (V_L > 12.2 kg/m^{2}s), nonuniform pulsing was observed (see Figure 14A). Pressure signals indicate that, at high liquid flow rates, one big pulse is associated with secondary small pulses. Up to $V_L = 15$ kg/m^{2}s, from PSD one primary and one secondary dominant frequency was observed and above $V_L = 15$ kg/m^{2}s (see Figure 14B). Characteristic frequencies of such pulses at different liquid flow rates are reported in Table 3. This information of natural pulse flow was used to specify appropriate inlet boundary conditions for the CFD model. The simulations of liquid-induced periodic operation were carried out for different liquid flow rates ($V_L = 11-24$ kg/m^{2}s) at a gas flow rate of $V_G = 0.22$ m/s.

At lower liquid flow rate of $V_L = 11$ kg/m^{2}s, observed natural pulse frequency of 1.56 Hz was specified as an input parameter for a liquid-induced periodic flow model. The simulations for periodic operation were carried out using interphase drag coupling terms similar to those used for a trickle flow regime. For this case, the predicted pressure drop was within 20% of the observed pressure drop. Predicted liquid holdup variation with time along the length of the column is shown in Figure 14C. At higher liquid flow rates (with nonuniform pulsing) the predicted pressure drop was lower than the observed pressure drop. The predicted liquid holdup contours for uniform and nonuniform periodic flows are shown in Figure 14D. To examine the possible influence of induced pulsing frequency, simulations were carried out at two different frequencies, i.e., 0.97 and 2.92 Hz at $V_L = 20$ kg/m^{2}s. Contours of simulated liquid holdup at these two pulsing frequencies are shown in Figures 14C and 14D, respectively. Interestingly the predicted pressure drop for these two frequencies was within 1%. Thus, hydrodynamics of periodic operation of trickle beds was not found to be sensitive to the exact value of induced pulsing frequency.

The approach, models, and results discussed here can provide a useful basis for further work on extending CFD models for simulating trickle-bed reactors.

Conclusions

In this study, we have experimentally and computationally investigated hydrodynamics of trickle beds. Experiments were carried out to study the effect of column and particle diameter on hydrodynamics for prewetted and non-prewetted bed conditions for a range of operating conditions ($V_G = 0.22-0.44$ kg/m^{2}s, $V_L = 2-24$ kg/m^{2}s).

Wall pressure fluctuations were measured and analyzed for accurate identification of transition from trickle to pulse flow regime and information on pulse frequency distribution. A comprehensive CFD model was developed to predict measured hydrodynamic parameters. The model was evaluated by comparing with the experimental data. A new method is proposed to predict frictional pressure drop and fraction of liquid holdup suspended in the form of drops using the developed CFD model. The CFD model was then extended to understand hydrodynamics predictions of trickle beds with periodic operation. The key findings of this study are as follows:

a. Kolmovgorov entropy calculated based on wall pressure fluctuations can accurately identify transition from trickle to pulse flow regime. The technique is nonintrusive and is applicable over a wide range of operating conditions.

b. Analysis of time series data provides valuable information about characteristic pulse frequencies. At low liquid flow rates ($V_L = 11-12.2$ kg/m^{2}s), a single dominant frequency indicating a uniform pulse rate was observed. At higher liquid flow rates ($V_L > 12.2$ kg/m^{2}s), two or three different frequencies of pulses were observed.

c. Time-averaged pressure drop and liquid holdup showed hysteresis with respect to liquid velocity. Observed hysteresis in pressure drop and liquid holdup for the 3 mm particles was larger compared to the 6 mm particle.

d. The spray distributor was found to perform better than the plate distributor and showed lower hysteresis.

e. The computational model developed in this work showed reasonable agreement with the experimental data for the prewetted beds. The model was also able to capture the trends observed in hysteresis correctly. However, quantitative predictions of hysteresis were lower than experimentally observed values. This highlights the need for further research on development of better capillary models.

f. The proposed method of simulating trickle-bed performance at two values of gravitational acceleration was able to estimate liquid holdup supported by gas. The approach can be used to identify existence and to quantify extent of spray regime in trickle beds.

g. Simulations with induced periodic flow indicated that predicted pressure drop is insensitive to the exact value of induced pulsing (within the range investigated in this work). Simulations of periodic flow through trickle beds can be used to understand some of the key features of natural pulse flow regime. The approach will also be useful to evaluate capillary models.

Acknowledgment

One of the authors (P.R.G.) is grateful to the Council of Scientific and Industrial Research (CSIR), India, for providing a senior research fellowship and to Prof V. G. Rao of IIT Bombay, for his valuable guidance. Authors wish to acknowledge financial support by the Department of Science and Technology Grant (No. DST/SF/40/99).

Appendix: Methodology for Calculating Static Head on the Gas Phase

For gas−liquid co-current down flow in trickle-bed reactors, we propose to use the following equation to relate the observed pressure drop and frictional pressure drop for the gas phase

$$\left(\frac{\Delta P}{L}\right)_{GL} = \left(\frac{\Delta P_f}{L}\right)_{GL} - (\rho_L \phi_L g)\phi_L \le \beta_L \qquad \text{(A.1)}$$

where β_L is the total liquid saturation and ϕ_L is the liquid saturation supported by the gas phase. Contribution of the gas-phase density in the static head component is neglected in eq A.1. If none of the liquid is supported by the gas phase, the value of ϕ_L becomes zero. Most of the authors have used such a formulation and have equated observed pressure drop with frictional pressure drop for the gas phase. In the other extreme, some authors have assumed that all of the liquid is supported by the gas phase and equated the value of ϕ_L to β_L (for example, Turpin and Huntington[48]). Both of these models allow calculation of frictional pressure drop from the experimentally measured values of overall pressure drop and total liquid saturation. The behavior of trickle-bed reactors is more likely to be between these two representations. That means the packed bed would support part of the liquid and part of the liquid may contribute to the static head. However, this intermediate behavior leads to two unknowns (frictional pressure drop and ϕ_L) in eq A.1.

To estimate these two unknown variables of interest, measurement of net pressure drop across the bed is not sufficient and it is necessary to devise alternative ways. The most obvious way to obtain these two unknowns is to carry out experimental measurements at two values of gravitational acceleration (say, g_1 and g_2). If these two values of gravitational acceleration are not very different, the overall pressure drop, frictional pressure drop, and liquid saturation may be assumed to be the same for these two sets of experiments. In such a case, the desired two unknown variables may be obtained as

$$\left(\frac{\Delta P_f}{L}\right) = \frac{g_1\left(\frac{\Delta P}{L}\right)_2 - g_2\left(\frac{\Delta P}{L}\right)_1}{g_1 - g_2} \qquad \text{(A.2)}$$

$$\phi_L = \frac{\left(\frac{\Delta P}{L}\right)_2 - \left(\frac{\Delta P}{L}\right)_1}{\rho_L(g_1 - g_2)} \qquad \text{(A.3)}$$

It is, however, rather difficult to carry out pressure drop measurements in a trickle-bed reactor under different values of gravitational acceleration. If an appropriate computational model is available to simulate gas−liquid flow through a packed bed, it is easier to carry out numerical experiments for two different values of gravitational acceleration. In this work, we have developed a comprehensive CFD model and have simulated gas−liquid flows in trickle-bed reactors at two values of gravitational acceleration (9.7 and 9.9 m/s^2) under different operating conditions. Since the difference in these two values of gravitational acceleration is small, the overall pressure drop, frictional pressure drop, and liquid saturation is not expected to vary significantly and, therefore, eqs A.2 and A.3 were used to estimate the frictional pressure drop, overall, and supported liquid saturation in trickle-bed reactors.

Nomenclature

a, b = constants defined in eq 2
d_1, d_2 = diameter of liquid film flowing over sphere, m

D = diameter of bed, m
d_p = particle diameter, m
E_1, E_2 = Ergun's constants
F = moment exchange coefficients, kg/m^{2}s
g = acceleration due to gravity, m/s^2
J_0 = zeroth-order Bessel function
L = length of the bed, m
P = pressure, N/m^2
$(\Delta P/L)$ = pressure drop per unit length, N/m^3
$(\Delta P_f/L)$ = friction pressure drop per unit length, N/m^3
$(\Delta P_f/L)_{GL}$ = two-phase frictional pressure drop, N/m^3
r = radius of column
t = time, s
U = interstitial velocity, m/s
V_G = gas mass velocity, kg/m^2/s, or superficial velocity, m/s
V_L = liquid mass velocity, kg/m^2/s, or superficial velocity, m/s

Greek Symbols

β = liquid saturation
ϵ_P = porosity in the jth cell
ϵ_B = average porosity of bed
ϵ_k = volume fraction of kth phase
$\epsilon(r)$ = axially averaged bed porosity at radius r
ϵ_S = solid volume fraction
ϵ = voidage
ϕ = liquid saturation supported by gas
ρ = density, kg/m^3
σ = surface tension, N/m
μ_k = viscosity of phase k in the bed, Pa s

Subscripts

G = gas phase
k = kth phase
L = liquid phase
R = phase other than k

Literature Cited

(1) Sie, S. T.; Krishna, R. Process Development and Scale Up, III: Scale up and scale down of trickle bed processes. *Rev. Chem. Eng.* **1998**, *14* (3), 203.

(2) Latifi, M.A.; Rode, S.; Midoux, N.; Storck, A The use of microelectrodes for the determination of flow regimes in a trickle-bed reactor. *Chem. Eng. Sci.* **1992**, *47*, 1955.

(3) Latifi, M. A.; Rode, S.; Midoux, N.; Storck, A. Hydrodynamic study of a trickle-bed reactor by means of microelectrodes: analysis of the probability densities. *Chem. Eng. Sci.* **1992**, *47*, 2331.

(4) Drahos, J.; Zahradnik, J.; Puncochar, M.; Flalova, M.; Bradka, F. Effect of operating conditions on the characteristics of pressure fluctuations in a bubble column. *Chem. Eng. Process.* **1991**, *29*, 197.

(5) Letzel H. M.; Schouten J. C.; Krishna R.; van den Bleek C. M. Characterization of regimes and regime transitions in bubble columns by chaos analysis of pressure signals. *Chem Eng. Sci*. **1997**, *52,* 4447.

(6) Lin, T. J.; Juang, R. C.; Chen, Y. C.; Chen, C. C. Predictions of flow transitions in a bubble column by chaotic time series analysis of pressure fluctuations signals. *Chem. Eng. Sci.* **2001**, *56*, 1057.

(7) Krieg, D. A.; Helwick, J. A.; McCready, M. J. Origin of disturbances in cocurrent gas−liquid packed bed flows. *AIChE J*. **1995**, *41* (7) 1653.

(8) Horowitz, G. I.; Cukierman, A. L.; Cassanello, M. A. Flow regime transition in trickle beds packed with particles of different wetting characteristics- check-up on new tool. *Chem. Eng. Sci.* **1997**, *52*, 3747.

(9) Urseanu, M. I.; Boelhouwer, J. G.; Bosmanand, H. J. M.; Schroijen, J. C. Induced pulse operation of high-pressure trickle bed reactors with organic liquids: hydrodynamics and reaction study. *Chem. Eng. Process.* **2004**, *43* (11)*,* 1411.

(10) Al-Dahhan, M. H.; Dudukovic, M. P. Pressure drop and liquid holdup in high-pressure trickle-bed reactors. *Chem. Eng. Sci.* **1994**, *49* (24), 5681.

(11) Saez, A. E.; Carbonell, R. G. Hydrodynamic parameters for gas liquid cocurrent flow in packed beds. *AIChE J.* **1985**, *31*, 52.

(12) Herskowitz, M.; Smith, J. M. Trickle Bed Reactors: A Review. *AIChE. J.* **1983**, *29*, 1.

(13) Kan, K. M.; Greenfield, P. F. Multiple hydrodynamic states in cocurrent two phase down flow through packed beds. *Ind. Eng. Chem. Process Des. Dev*. **1978**, *17*, 482.

(14) Kan, K. M.; Greenfield, P. F. Pressure drop and hold up in two phase cocurrent trickle flows through beds of small particles, *Ind. Eng. Chem. Process Des. Dev*. **1979**, *18*, 740.

(15) Christensen, G.; Sundaresan, S.; McGovern, S. J. Co-current downflow of air and water in a two-dimensional packed column. *AIChE J.* **1986**, *32* (10), 1677−1689.

(16) Levec, J.; Grosser, K.; Carbonell, R. G. The hysteretic behavior of pressure drop and liquid hold up in trickle beds. *AIChE J.* **1988**, *34*, 1027.

(17) Levec, J.; Saez, A. E.; Carbonell, R. G. The hydrodynamics of trickling flow in packed beds, Part II: Experimental observations. *AIChE J.* **1986**, *32*, 369.

(18) Rode, S.; Midoux, N.; Latifi, M. A.; Storck, A. Multiple hydrodynamic states in trickle beds operating in high interaction regimes: liquid saturation and flow regime transitions. *Chem. Eng. Sci.* **1994**, *49*, 2535.

(19) Chu, C. F.; Ng, K. M. Model for pressure drop hysteresis in trickle beds. *AIChE J.* **1989***, 35*, 1677.

(20) Ravindra, P. V.; Rao, D. P.; Rao, M. S. Liquid flow texture in trickle bed reactors: an experimental study. *Ind. Eng. Chem. Res.* **1997**, *36*, 5133.

(21) Melli, T. R.; Scriven, L. E. Theory of two phase cocurrent downflow in networks of passages. *Ind. Eng. Chem. Res*. **1991**, *30*, 951.

(22) Attou, A.; Ferschneider, G. A two-fluid hydrodynamic model for the transition between trickle and pulse flow in a cocurrent gas−liquid packed-bed reactor. *Chem. Eng. Sci.* **2000**, *55*, 491.

(23) Jiang, Y.; Khadilkar M. R.; Al-Dahhan, M. H.; Dudukovic, M. P. CFD modeling of multiphase in packed bed reactors: results and applications. *AIChE J.* **2002**, *48*, 716.

(24) Iliuta, I.; Larachi, F.; Iliuta, M. C.; Grandjean, B. P. A.; Hydrodynamic continuum model for gas−liquid fixed beds operating in trickle flow and pre-loading regimes. *Chem. Eng. Res., Des*. **2002**, *80* (A7), 790.

(25) Souadnia, A.; Latifi, M. A. Analysis of two-phase flow distribution in trickle-bed reactors. *Chem. Eng. Sci*. **2001**, *56* (21−22), 5977.

(26) Gunjal, P. R.; Ranade, V. V.; Chaudhari, R. V. Liquid-phase residence time distribution in trickle bed reactors: Experiments and CFD simulations. *Can. J. Chem. Eng.* **2003**, *81*, 821.

(27) Jiang, Y. Flow distribution and its impact on performance of packed-bed reactors. Ph.D. Thesis, Washington University, St. Louis, MO, Dec 2000.

(28) Mantle, M. D.; Sederman, A. J.; Gladden, L. F. Single and two-phase flow in fixed-bed reactors: MRI flow visualization and lattice-Boltzmann simulation. *Chem. Eng. Sci.* **2001**, *56,* 523.

(29) Stephenson, J. L.; Stewart, W. E. Optical measurements of porosity and fluid motion in packed beds. *Chem. Eng. Sci.* **1986**, *41*, 2161.

(30) Spedding, P. L.; Spencer, R. M. Simulation of packing density and liquid flow in fixed beds. *Comput. Chem. Eng.* **1995**, *19*, 43.

(31) Mueller, G. E. Prediction of radial porosity distribution in randomly packed fixed beds of uniformly sized spheres in cylindrical containers. *Chem. Eng. Sci.* **1991**, *46*, 706.

(32) Crine, M.; Marchot, P.; L'Homme, G. A. Mathematical modeling of the liquid trickling flow through a packed bed using the percolation theory. *Comput. Chem. Eng.* **1979**, *3*, 515.

(33) Thompson, K. E.; Fogler, H. S. Modeling flow in disordered packed beds from pore-scale fluid mechanics. *AIChE J.* **1997**, *43* (6), 1377.

(34) Yin, F. H.; Sun, C. G.; Afacan, A.; Nandakumar, K.; Chung, K. T. CFD Modeling of Mass-Transfer Processes in Randomly Packed Distillation Columns. *Ind. Eng. Chem. Res.* **2000**, *39*, 1369.

(35) Attou, A.; Ferschneider, G. A. Two-fluid model for flow regime transition in gas−liquid trickle-bed reactors. *Chem. Eng. Sci.* **1999**, *54* (21), 5031.

(36) Grosser, K.; Carbonell, R. G.; Sundaresan, S. Onset of pulsing in two-phase concurrent downflow through a packed bed. *AIChE J.* **1988**, *34*, 185.

(37) Kashiwa, B. A.; Padial, N. T.; Rauenzahn, R. M.; VanderHeyden, W. B. A cell centered ICE method for multiphase flow simulations. *ASME Symposium on Numerical Methods for Multiphase Flows*, Lake Tahoe, NV, 1994.

(38) Ranade, V. V. *Computational flow modeling for chemical reactor engineering*; Academic Press: London, 2000.

(39) Holub, R. A.; Dudukovic, M. P.; Ramachandran, P. A. A phenomenological model for pressure drop, liquid holdup, and flow regime transition in gas−liquid trickle flow. *Chem. Eng. Sci.* **1992**, *47* (9−11), 2343.

(40) Holub, R. A.; Dudukovic, M. P.; Ramachandran, P. A. Pressure drop, liquid hold-up and flow regime transition in trickle flow. *AIChE J.* **1993**, *39*, 302.

(41) Szady, M. J.; Sundaresan, S. Effect of boundaries on trickle bed hydrodynamics. *AIChE J.* **1991**, *37*, 1237.

(42) Schouten, J. C.; Takens, F.; Van den Bleek, C. M. Estimation of the dimension of a noisy attractor. *Phys. Rev. E* **1994**, *49*, 126.

(43) Ranade, V. V.; Utikar, R. P. Dynamics of gas−liquid flows in bubble column reactors. *Chem. Eng. Sci.* **1999**, *54*, 5237.

(44) Wang, Y.-F.; Mao, Z.-S.; Chen, J.-Y. Experimental and theoretical studies of pressure drop hysteresis in trickle bed reactors. *Chem. Eng. Sci.* **1995**, *50* (14), 2321.

(45) Rao, V. G.; Ananth, M. S.; Varma, Y. B. G. Hydrodynamics of two phase cocurrent downflow through packed beds. *AIChE J.* **1983**, *29* (3), 467.

(46) Specchia, V.; Baldi, G. Pressure drop and liquid hold up for two phase cocurrent flow in packed bed. *Chem. Eng. Sci*. **1977**, *32*, 515.

(47) Boelhouwer, J. G.; Piepers H. W.; Drinkenburg, A. A. H. Liquid-induced pulsing flow in trickle-bed reactors. *Chem. Eng. Sci*. **2002,** *57*, 3387.

(48) Turpin, J. L.; Huntington, R. L. Prediction of pressure drop for two phase, two component cocurrent flow in packed beds. *AIChE J.* **1967**, *13*, 1196.

Received for review September 15, 2004
Revised manuscript received January 17, 2005
Accepted January 20, 2005

IE0491037